Electronic Supplementary Material (ESI) for Faraday Discussions.

Supporting Information for:

Thermodynamic exploration of xenon/krypton separation based on a high-throughput screening

Emmanuel Ren†,‡ and François-Xavier Coudert†

†*Chimie ParisTech, PSL University, CNRS, Institut de Recherche de Chimie Paris, 75005 Paris, France*

‡*CEA, DES, ISEC, DMRC, University of Montpellier, Marcoule, F-30207 Bagnols-sur-Cèze, France*

Exchange equilibrium

$$\mathrm{Xe}_{(g)} + \mathrm{Kr}_{(ads)} = \mathrm{Xe}_{(ads)} + \mathrm{Kr}_{(g)}$$

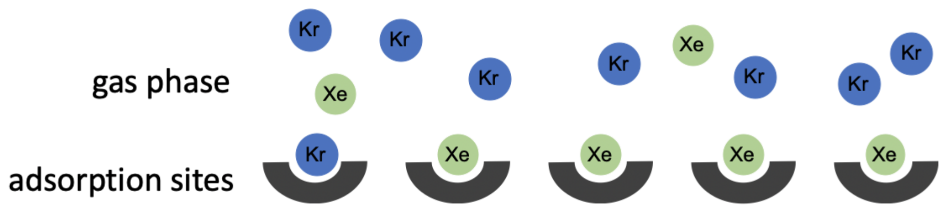

Figure S1: Representation of the fictitious exchange equilibrium between xenon and krypton considered in our study.

Other correlations

It is possible to define an entropy of adsorption of a guest g for a given standard state (P°=1 atm):

$$\Delta_{\mathrm{ads}} S_0^{\mathrm{g}} = R \ln\left(P^{\circ} M^{\mathrm{f}} K^{\mathrm{g}}\right) + \frac{1}{T} \Delta_{\mathrm{ads}} H_0^{\mathrm{g}} \tag{S1}$$

where R is the ideal gas constant, T is the temperature equals to 298 K, P° is the pressure at atmospheric pressure and M_{f} is the framework's molar mass in g mol^{-1}, K^{g} the Henry's constant of g and $\Delta_{\mathrm{ads}} H_0^{\mathrm{g}}$ the adsorption enthalpy of g.

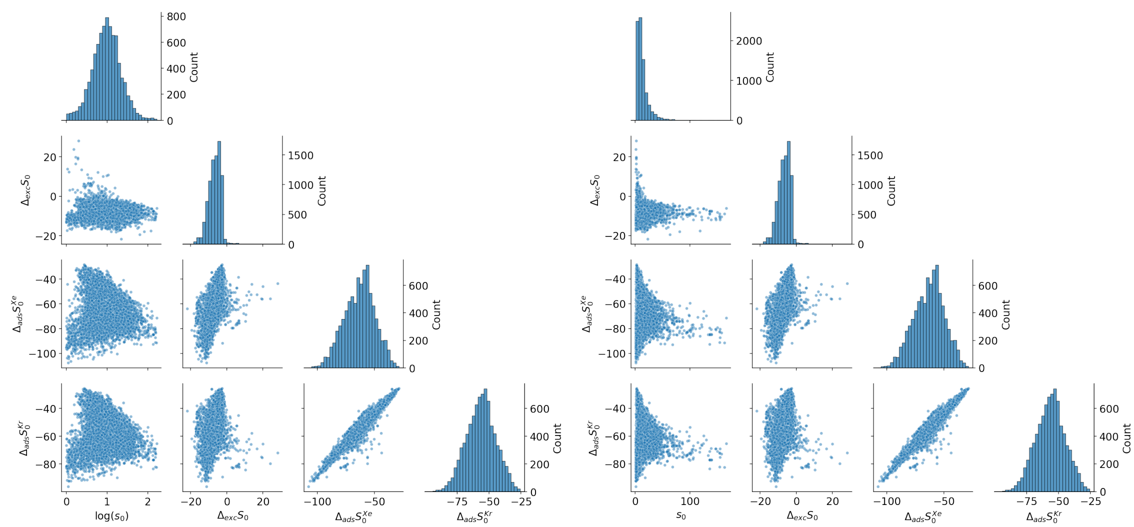

Figure S2: Entropy pair-plots in both linear and log scale.

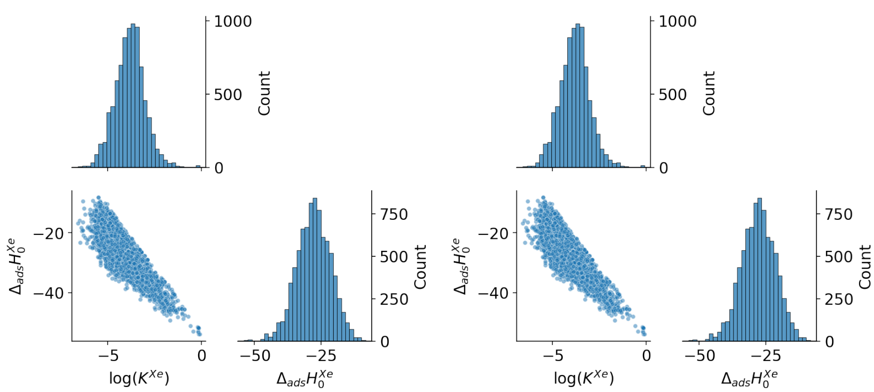

Figure S3: Correlation between henry coefficient and enthalpy for both xenon and krypton

Difference of selectivity: the 90:10 composition case

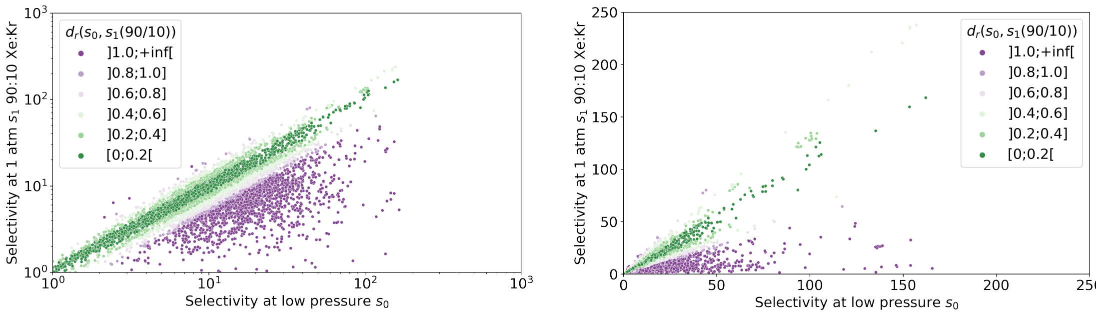

Figure S4: Overview at linear and log scale, comparison between s_0 and $s_1(90:10)$

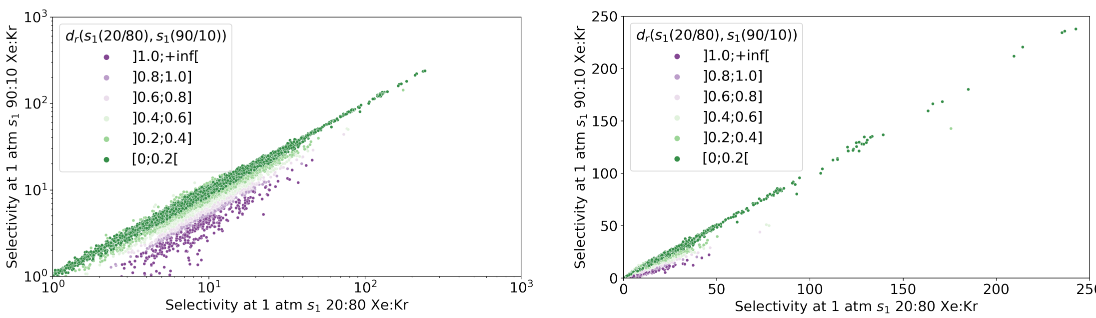

Figure S5: Overview at linear and log scale, comparison between $s_1(20:80)$ and $s_1(90:10)$

Entropy and enthalpy between low an high selectivity

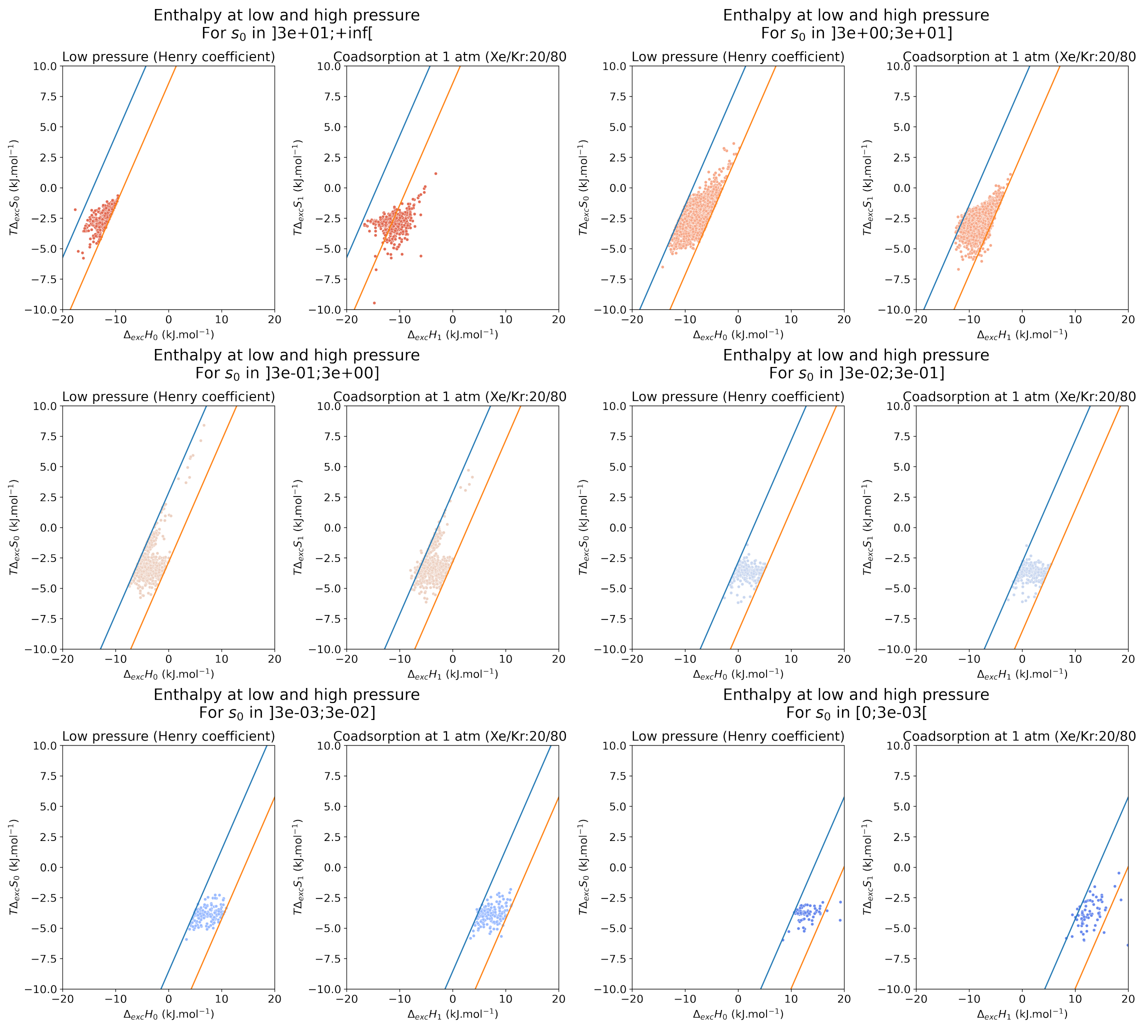

Figure S6: Split view of the figures 4 and 5 of the article. The iso-selectivity lines for the limit considered are represented with blue and orange lines.

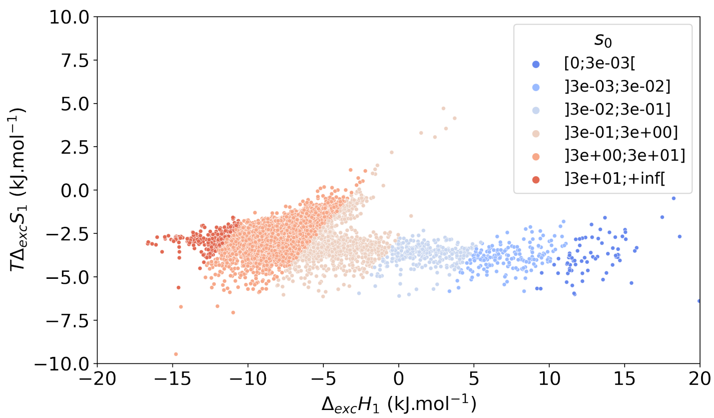

Figure S7: The energetic equivalent of exchange equilibrium entropy $T\Delta_{\text{exc}}S_1$ and enthalpy $\Delta_{\text{exc}}H_1$ at ambient pressure labeled using the selectivity s_1 at ambient pressure.

Distribution of the exchange enthalpy and entropy

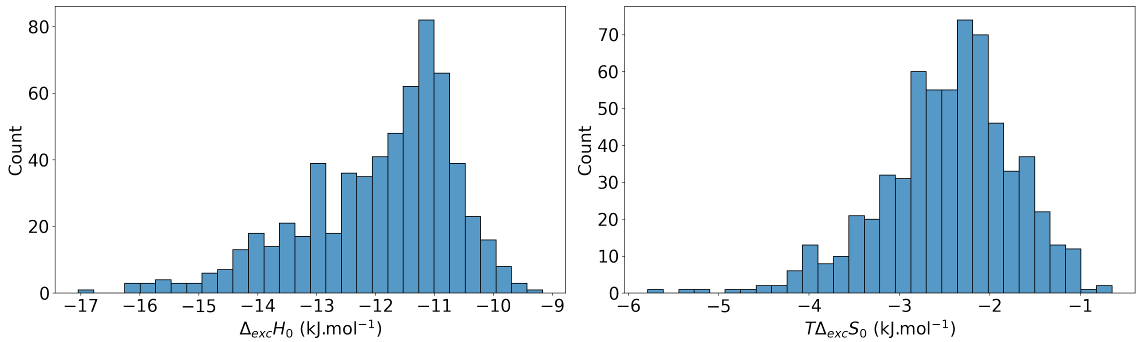

Figure S8: Distribution of the enthalpy and entropy of exchange at low pressure on the 630 most selective structures

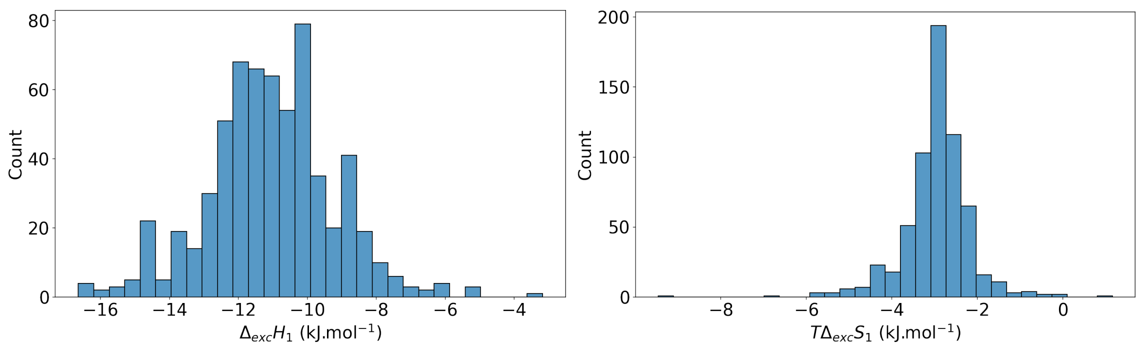

Figure S9: Distribution of the enthalpy and entropy of exchange at ambient pressure on the 630 most selective structures

Raw data for the archetypal structures presented in the main article

Table S1: Raw thermodynamic quantities associated for a few representative examples of MOFs. Henry's constant K^{Xe}, K^{Kr} are in mmol g^{-1} Pa^{-1}, loadings q_1^{Xe} and q_1^{Kr} are in mmol g^{-1}, enthalpies $\Delta_{\mathrm{ads}}H_0^{\mathrm{Xe}}$, $\Delta_{\mathrm{ads}}H_0^{\mathrm{Xe}}$, $\Delta_{\mathrm{ads}}H_1^{\mathrm{Xe}}$ and $\Delta_{\mathrm{ads}}H_1^{\mathrm{Xe}}$ are in kJ mol^{-1}, and diameters D_{i} and D_{f} in Å

CSD Refcode	s_0	K^{Xe}	K^{Kr}	$\Delta_{\mathrm{ads}}H_0^{\mathrm{Xe}}$	$\Delta_{\mathrm{ads}}H_0^{\mathrm{Kr}}$	s_1	q_1^{Xe}	q_1^{Kr}	$\Delta_{\mathrm{ads}}H_1^{\mathrm{Xe}}$	$\Delta_{\mathrm{ads}}H_1^{\mathrm{Xe}}$	D_{i}	D_{f}
VOKJIQ	157	$7.92\,10^{-1}$	$5.04\,10^{-3}$	−53.9	−38.2	243	2.57	0.04	−61.1	−44.5	4.8	2.9
KAXQIL	104	$3.01\,10^{-2}$	$2.90\,10^{-4}$	−44.6	−30.5	133	1.41	0.04	−41.5	−26.8	5.1	3.8
JUFBIX	106	$1.59\,10^{-2}$	$1.50\,10^{-4}$	−45.6	−31.4	115	0.80	0.03	−45.7	−31.3	5.0	2.7
FALQOA	162	$2.23\,10^{-2}$	$1.38\,10^{-4}$	−47.3	−32.0	171	0.68	0.02	−48.6	−33.1	5.1	3.1
GOMREG	114	$9.16\,10^{-2}$	$8.03\,10^{-4}$	−44.7	−31.1	74	2.59	0.14	−47.5	−33.8	5.4	3.6
JAVTAC	117	$1.24\,10^{-1}$	$1.06\,10^{-3}$	−47.7	−33.5	67	1.50	0.09	−48.5	−34.9	5.1	3.9
GOMRAC	124	$1.17\,10^{-1}$	$9.45\,10^{-4}$	−45.6	−31.8	47	2.51	0.21	−47.3	−34.8	5.3	3.4
MISQIQ	139	$6.87\,10^{-1}$	$4.94\,10^{-3}$	−51.9	−37.4	37	2.30	0.25	−45.6	−32.8	4.2	4.1
BAEDTA01	154	$1.39\,10^{-2}$	$9.04\,10^{-5}$	−47.7	−31.7	38	1.05	11	−34.0	−23.1	5.3	4.3
VIWMOF	81	$7.87\,10^{-3}$	$9.70\,10^{-5}$	−46.3	−30.1	13	2.99	0.90	−26.0	−17.8	9.8	5.2
LUDLAZ	166	$9.04\,10^{-2}$	$5.46\,10^{-4}$	−45.4	−30.9	16	1.59	0.39	−38.3	−28.3	6.6	4.2
WOJJOV	146	$4.19\,10^{-2}$	$2.86\,10^{-4}$	−46.4	−30.7	14	2.82	0.81	−33.0	−24.4	7.8	6.4
VAPBIZ	147	$3.54\,10^{-2}$	$2.41\,10^{-4}$	−46.4	−30.5	13	2.50	0.78	−34.1	−25.3	6.3	3.6

Lennard-Jones (LJ) potentials The van der Waals interaction can be approximately modeled by the following potential V_{LJ}:

$$V_{\mathrm{LJ}} = 4\varepsilon\left(\left(\frac{\sigma}{r}\right)^{12} - \left(\frac{\sigma}{r}\right)^{6}\right) \tag{S2}$$

where ε is the depth of the well (minimal energy), σ is the distance from which the interaction becomes stabilizing and r is the distance between the two interacting atoms.

Lorentz-Berthelot rules From LJ parameters of interactions between the same type of atoms we can determine interactions between different types of atoms:

$$\begin{aligned} \varepsilon_{\mathrm{ij}} &= \sqrt{\varepsilon_{\mathrm{ii}} \times \varepsilon_{\mathrm{jj}}} \\ \sigma_{\mathrm{ij}} &= \frac{\sigma_{\mathrm{ii}} + \sigma_{\mathrm{jj}}}{2} \end{aligned} \tag{S3}$$

where i and j are indexes corresponding to two different types of atoms (e.g., i=Xe and j=Kr)

Langmuir 1-site At given temperature, some mono-site materials' isotherm can be described by the following equation:

$$q(P) = N_{\max} \frac{KP}{1+KP} \tag{S4}$$

where q is the loading of a given mono-component gas, K is the adsorption equilibrium constant and P is the pressure.

Langmuir 2-site At given temperature, some two-site materials' isotherm can be described by the following equation:

$$q(P) = N_{\max} \left((1-\alpha_2) \frac{K_1 P}{1+K_1 P} + \alpha_2 \frac{K_2 P}{1+K_2 P} \right) \tag{S5}$$

where q is the loading of a given mono-component gas, K_1 and K_2 are the adsorption equilibrium constants in the respective sites, α_2 is the proportion of secondary sites, and P is the pressure.

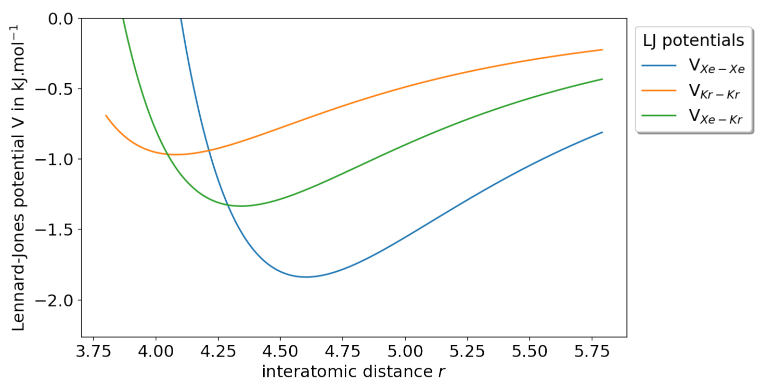

Figure S10: The LJ potentials for xenon and krypton interactions. The xenon-xenon interaction is more stabilizing than the krypton-krypton interaction for inter-atomic distance higher than 4.2 Å.

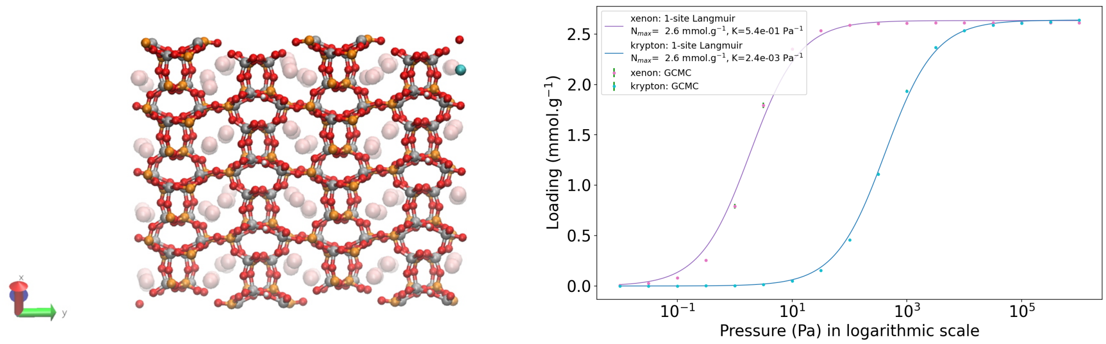

Figure S11: VOKJIQ: On the left side, an illustration of a clean version (all solvent removed) of the open-framework aluminophosphate $[HAl_3P_3O_{13}]\cdot C_3NH_{10}$ loaded with xenon and krypton obtained by GCMC calculations. Color code: Al in silver, P in orange, O in red, H in white ; Xe in transparent pink and Kr in cyan for the adsorbates. The mono-component isotherms fitted with a 1-site Langmuir model for both xenon and krypton at 298 K is represented on the right side.

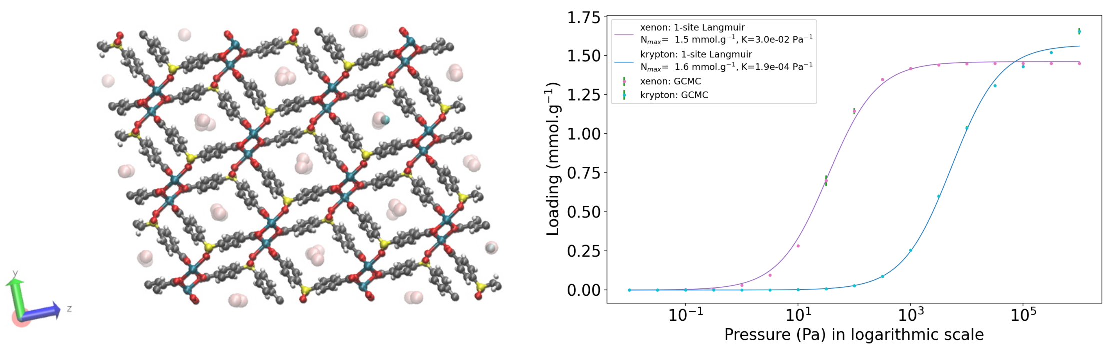

Figure S12: KAXQIL: On the left side, an illustration of a clean version (all solvent removed) of the calcium coordination framework $[Ca(SDB)]\cdot H_2O$, where SDB = 4,4′-sulfonyldibenzoate loaded with xenon and krypton obtained by GCMC calculations. Color code: Ca in dark cyan, C in gray, O in red, H in white, S in yellow ; Xe in transparent pink and Kr in cyan for the adsorbates. The mono-component isotherms fitted with a 1-site Langmuir model for both xenon and krypton at 298 K is represented on the right side.

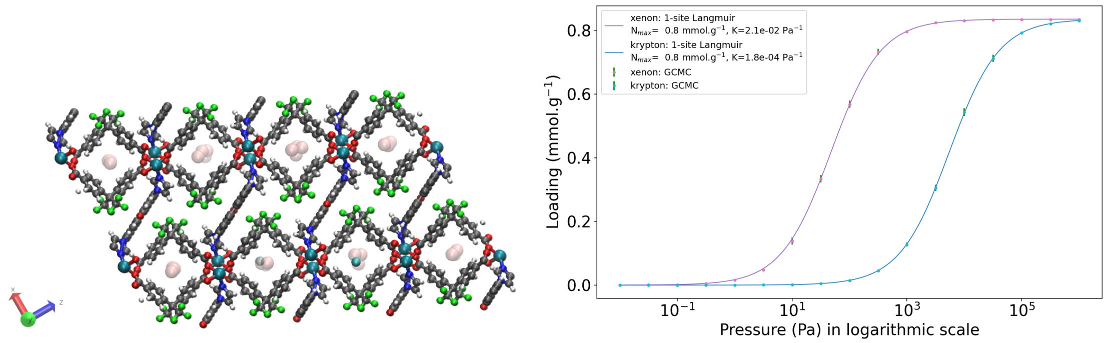

Figure S13: JUFBIX: Representation of a clean version (all solvent removed) of the cobalt(II) coordination framework $[Co_2(L)(ppda)_2]_2{\cdot}H_2O$, where the ligand L is 2,8-di(1*H*-imidazol-1-yl)dibenzofuran and the carboxylic acid ligand H_2ppda is 4,4′-(perfluoropropane-2,2-diyl)dibenzoic acid loaded with xenon and krypton obtained by GCMC calculations. Color code: Co in dark cyan, C in gray, O in red, H in white, N in blue, F in green ; Xe in transparent pink and Kr in cyan for the adsorbates. The mono-component isotherms fitted with a 1-site Langmuir model for both xenon and krypton at 298 K is represented on the right side.

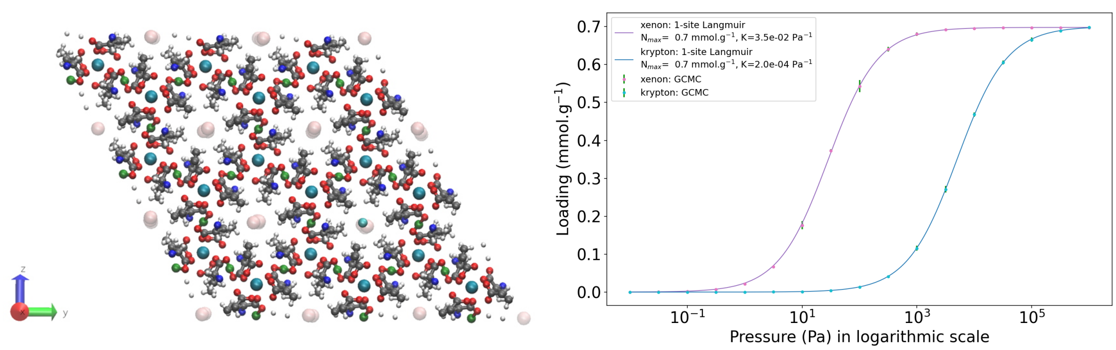

Figure S14: FALQOA: Representation of a clean version (all solvent removed) of the Nd-Cu heterometallic coordination polymer $[Nd_2Cu_3(ANMA)_6]{\cdot}3(H_2O)$, where the ligand ANMA is the deprotonated form of H_2ANMA = L-alanine-*N*-monoacetic acid loaded with xenon and krypton obtained by GCMC calculations. Color code: Cu in dark green, Nd in dark cyan, C in gray, O in red, H in white, N in blue ; Xe in transparent pink and Kr in cyan for the adsorbates. The mono-component isotherms fitted with a 1-site Langmuir model for both xenon and krypton at 298 K is represented on the right side.

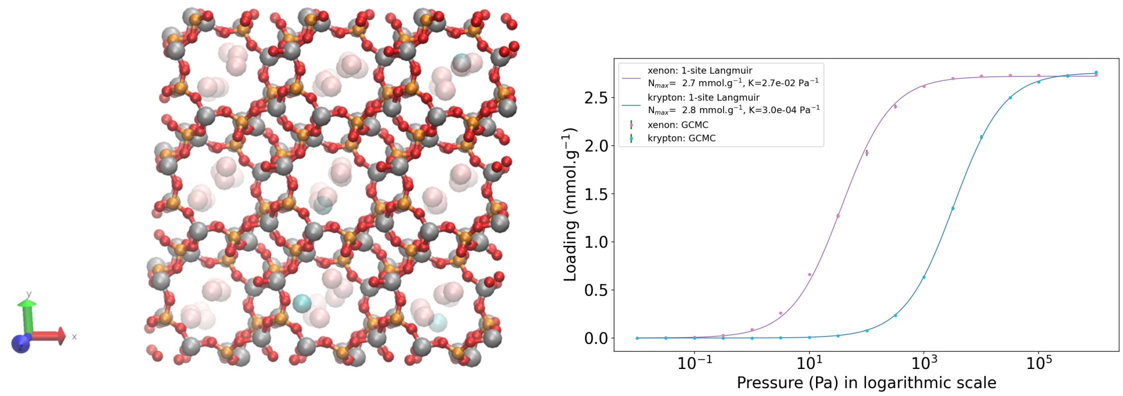

Figure S15: GOMREG: Representation of a clean version (all solvent removed) of this aluminophosphate $AlPO_4$-*n* that has a zeotype LAU topology with one-dimensional 10-ring channels loaded with xenon and krypton obtained by GCMC calculations. Color code: Al in silver, P in orange, O in red ; Xe in transparent pink and Kr in cyan for the adsorbates. The mono-component isotherms fitted with a 1-site Langmuir model for both xenon and krypton at 298 K is represented on the right side.

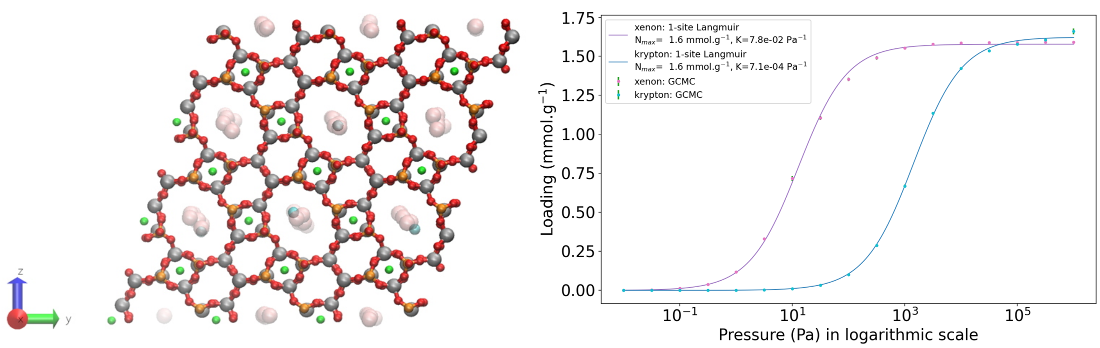

Figure S16: JAVTAC: Representation of a clean version (all solvent removed) of this open-framework fluoroaluminophosphate SIZ-3 $[Al_5P_5O_{20}F_2]\cdot 2(C_6H_{11}N_2)$ that has an AlPO-11 framework structure loaded with xenon and krypton obtained by GCMC calculations. Color code: Al in silver, P in orange, O in red, F in green ; Xe in transparent pink and Kr in cyan for the adsorbates. The mono-component isotherms fitted with a 1-site Langmuir model for both xenon and krypton at 298 K is represented on the right side.

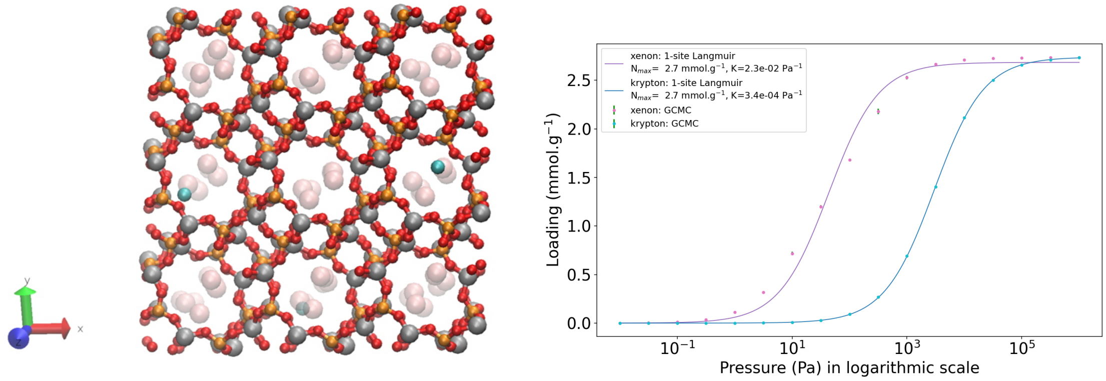

Figure S17: GOMRAC: Representation of a clean version (all solvent removed) of this aluminophosphate $AlPO_4$-*n* that has a zeotype LAU topology with one-dimensional 10-ring channels loaded with xenon and krypton obtained by GCMC calculations. Color code: Al in silver, P in orange, O in red ; Xe in transparent pink and Kr in cyan for the adsorbates. The mono-component isotherms fitted with a 1-site Langmuir model for both xenon and krypton at 298 K is represented on the right side. It seems that this aluminophosphate is just a smaller version of GOMREG.

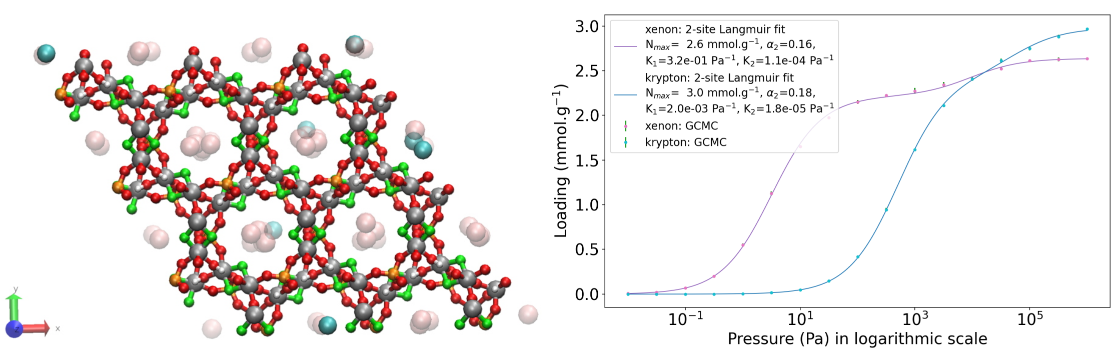

Figure S18: MISQIQ: Representation of a chiral open-framework fluoroaluminophosphate $[Al_6P_3O_{12}F_6(OH)_6]\cdot C_4N_3H_{16}$ denoted AlPO-JU89 on the left side. Color code: Al in silver, P in orange, O in red, H in white and F in green for the framework ; and Xe in transparent pink and Kr in cyan for the adsorbates. The mono-component isotherms fitted with a 2-site Langmuir model for both xenon and krypton at 298 K on the right side.

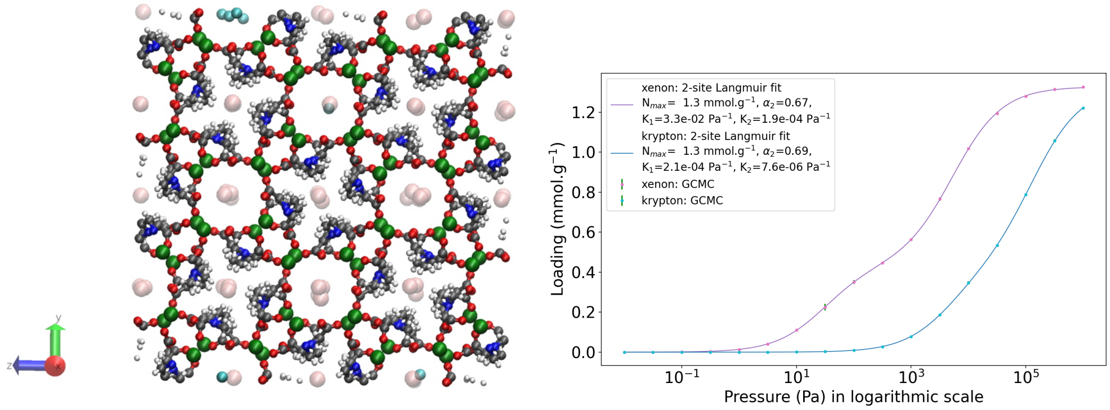

Figure S19: BAEDTA01: Representation of a baryum-based MOF [Ba_2(EDTA)]·2.5(H_2O), where EDTA is the deprotonated form of H_2EDTA = ethylenediaminetetraacetic acid, on the left side. Color code: Ba in dark green, C in gray, O in red, H in white, N in blue for the framework ; and Xe in transparent pink and Kr in cyan for the adsorbates. The mono-component isotherms fitted with a 2-site Langmuir model for both xenon and krypton at 298 K, on the right side.

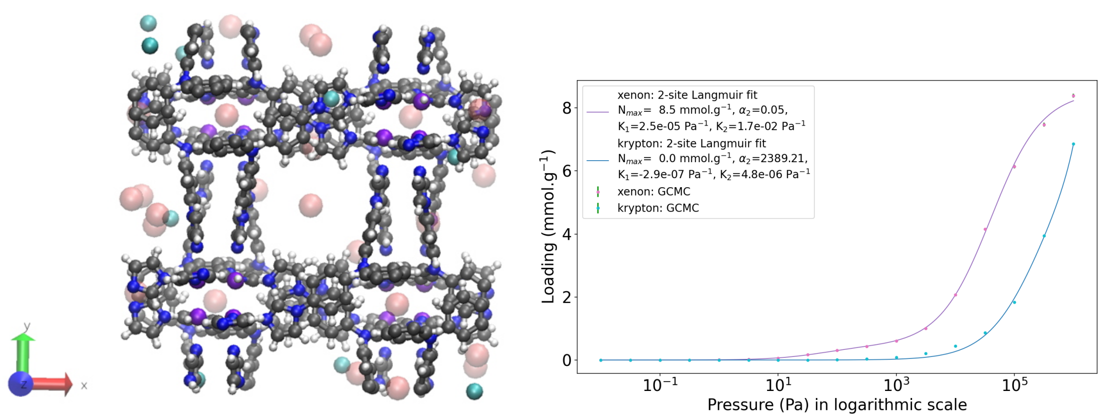

Figure S20: VIWMOF: Representation of a chiral cadmium-based MOF conglomerate [Cd(tipa)(μ_3-OH)]·NO_3·EtOH·DMF where tipa is tris(4-(1*H*-imidazol-1-yl)phenyl)amine and DMF is dimethylformamide, on the left side. Color code: Cd in dark pink, C in gray, H in white, N in blue for the framework ; and Xe in transparent pink and Kr in cyan for the adsorbates. The mono-component isotherms fitted with a 2-site Langmuir model for both xenon and krypton at 298 K, on the right side.

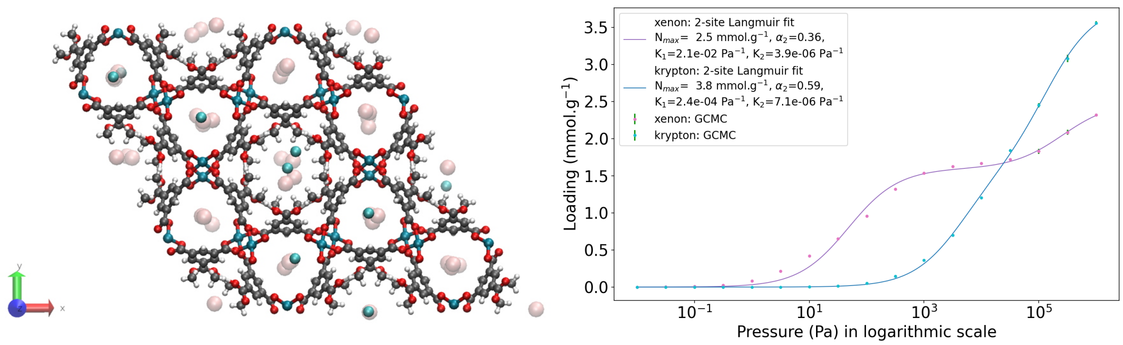

Figure S21: LUDLAZ: Representation of a copper-based MOF known as STAM-1 $[Cu_3O_{21}C_{30}H_{24}]\cdot 5(H_2O)$, on the left side. Color code: Cu in dark cyan, C in gray, O in red, H in white for the framework ; and Xe in transparent pink and Kr in cyan for the adsorbates. The mono-component isotherms fitted with a 2-site Langmuir model for both xenon and krypton at 298 K, on the right side.

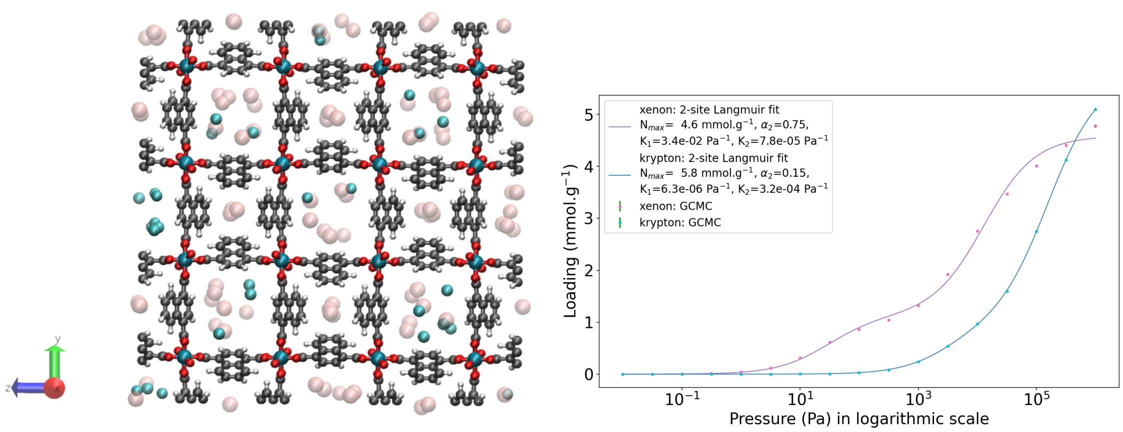

Figure S22: WOJJOV: Representation of an aluminium-based MOF $[Al(OH)(1,4\text{-}NDC)]\cdot 2(H_2O)$ where NDC means naphthalenedicarboxylate, on the left side. Color code: Cu in dark cyan, C in gray, O in red, H in white for the framework ; and Xe in transparent pink and Kr in cyan for the adsorbates. The mono-component isotherms fitted with a 2-site Langmuir model for both xenon and krypton at 298 K, on the right side.

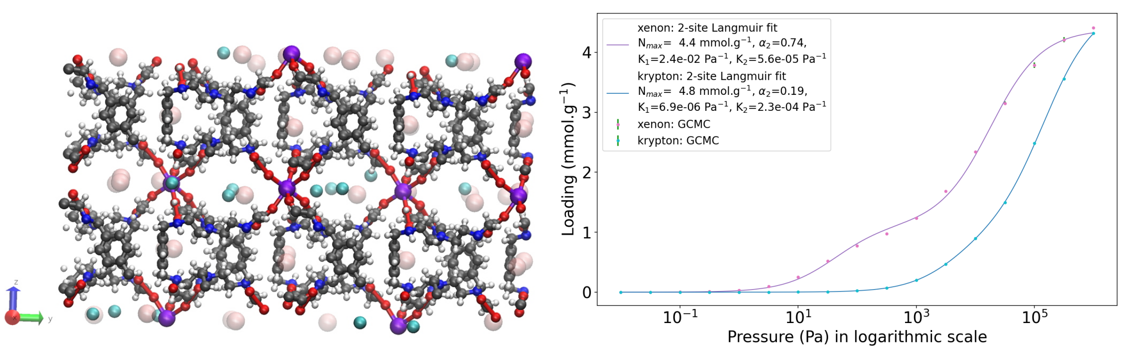

Figure S23: VAPBIZ: Representation of a europium-based homochiral MOF $[EuL(NO_3)_3(H_2O)]\cdot 13(H_2O)$ where L is an achiral hexacarboxylic ligand, on the left side. Color code: Cu in dark cyan, C in gray, O in red, H in white for the framework ; and Xe in transparent pink and Kr in cyan for the adsorbates. The mono-component isotherms fitted with a 2-site Langmuir model for both xenon and krypton at 298 K, on the right side.